超声冲击对转向架焊接十字接头表层组织及疲劳性能的影响

何柏林[1]， 于影霞[1]， 余皇皇[1]， 江民华[1]， 史建平[2]
(1. 华东交通大学 载运工具与装备教育部重点实验室，南昌 330013；2. 中国铁道科学研究院，北京 100081)

摘 要： 采用HJ2-Ⅱ型超声冲击机对转向架常用16MnR钢十字接头焊趾进行超声冲击处理. 采用高分辨透射电镜对冲击后的十字接头焊趾区域表面微观组织进行了分析，利用EHF-EM200K2-070-1A疲劳试验机对16MnR焊态和超声冲击态十字接头进行了疲劳性能的对比试验研究. 结果表明，超声冲击后在焊趾及其附近区域获得纳米化组织，超声冲击前后接头试样均断于焊趾；焊态十字接头的条件疲劳极限(2×10^6)为158 MPa，冲击态十字接头的条件疲劳极限(2×10^6)为236 MPa，条件疲劳极限提高了49%左右，接头的疲劳寿命延长了45～52倍. 超声冲击在提高16MnR十字接头疲劳性能方面具有显著的效果.

关键词： 十字接头；超声冲击；疲劳性能；S－N曲线；16MnR钢
中图分类号： TG457.11 **文献标识码：** A **文章编号：** 0253－360X(2013)08－0051－04

何柏林

0 序 言

接头焊趾及焊跟部位是焊接结构承受疲劳载荷的薄弱环节，改善焊趾和焊根部位的疲劳性能将提高整个结构的疲劳性能.

超声冲击处理(ultrasonic impact treatment，UIT)是近年来发展起来的一种改善焊接接头疲劳性能的新工艺，不同强度级别的钢种试验结果表明，UIT能显著改善焊接接头的疲劳性能[1-3]. 该方法由于执行重量轻、体积小、可控性好、效率高、噪音低、应用时受限少，而成为一种理想的焊后提高焊接接头疲劳性能的处理工艺[4].

在实际应用中，焊接转向架构架的破坏大多始于焊接接头. 这是因为焊接接头处气孔、夹渣等缺陷较多，应力集中系数大，容易产生裂纹并扩展，从而降低焊接转向架的疲劳强度和使用寿命. 国内外学者[5-8]对焊接转向架做了大量的研究，探索了各种因素对焊接接头疲劳性能的影响，并取得了显著的成绩. 文中采用超声冲击处理16MnR十字接头，研究超声冲击处理对焊趾区表面组织的细化作用以及超声冲击前后焊接接头疲劳性能的改善效果.

收稿日期： 2013－01－20
基金项目： 国家自然科学基金资助项目(51065010)；江西省自然科学基金资助项目(2009GZC0016)

1 试验方法

1.1 试验材料及接头形式

接头试样的几何形状和尺寸如图1所示. 试验材料为16MnR钢，母材力学性能见表1.

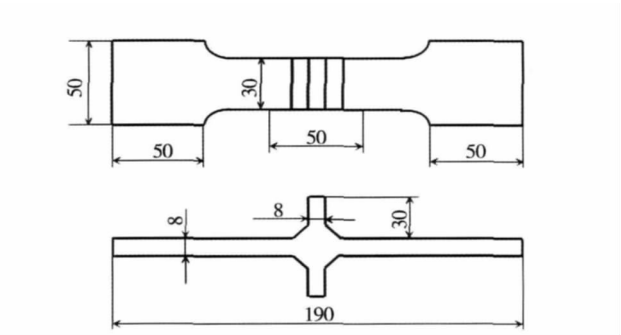

图1 十字接头几何形状和尺寸(mm)
Fig. 1 Shape and size of cross joints

表1 16MnR钢的常规力学性能
Table 1 Mechanical properties of 16MnR

屈服强度 R_{eL}/MPa	抗拉强度 R_m/MPa	断后伸长率 A(%)
360	580	27

1.2 超声冲击处理试验

冲击过程中超声冲击枪对准试样的焊趾部位，

基本垂直于焊缝，且冲击头的冲击针阵列沿焊缝方向排列. 略施加一定的压力，使处理过程中冲击枪基本在自重的条件下进行. 超声冲击处理时激励电流为 1.2 A，冲击枪对每道焊趾来回冲击处理 2 次.

1.3 超声冲击表面微观组织观察

采用高分辨透射电镜(HRTEM)对超声冲击后接头焊趾区域的表面微观组织进行分析，探讨超声冲击处理对接头焊趾区表面微观组织的影响及细化机理.

1.4 疲劳试验

焊接接头的疲劳试验在岛津电液伺服疲劳试验机上进行. 载荷类型为拉—拉载荷，应力比 $R = 0.1$，加载频率 $f = 10$ Hz. 将相同接头形式的试件分为两组，第一组不采用超声冲击处理；第二组进行超声冲击处理.

2 疲劳试验数据处理方法

根据国际焊接学会(IIW)钢结构循环加载疲劳文件的相关规定，采用下述统计方法对接头疲劳试验数据结果进行处理[9]. 该统计方法的前提条件是疲劳试验数据结果呈对数正态分布，国际焊接学会规定的数据存活率为 95%，置信度标称值为 75%.

标称值通过下述方法进行计算.

(1) 计算疲劳试验数据结果的应力范围 $\Delta\sigma$ 和疲劳寿命 N 换算成以 10 为底的对数值.

(2) 采用幂指函数回归模型计算指数 m 和常数 $\lg C$ 的值，即

$$m\lg\Delta\sigma + \lg N = \lg C \tag{1}$$

式中：m，C 为拟合常数.

(3) 设 C_i 是试验数据的对数值，利用所获得的 m 值，计算 $\lg C$ 的平均值 C_{m} 和标准偏差 $S_{\mathrm{td}\nu}$，即

$$C_{\mathrm{m}} = \frac{\sum C_i}{n} \tag{2}$$

$$S_{\mathrm{td}\nu} = \sqrt{\frac{\sum (C_{\mathrm{m}} - C_i)^2}{n-1}} \tag{3}$$

(4) 计算特征值 C_{k}，即

$$C_{\mathrm{k}} = C_{\mathrm{m}} - KS_{\mathrm{td}\nu} \tag{4}$$

3 试验结果

3.1 微观组织分析

图 2 为超声冲击处理表面组织的高分辨透射电镜明场像，选区电子衍射花样见图 3.

从图 2 可以看出，焊趾经超声冲击处理后，在 16MnR 钢焊接接头焊趾及其附近表面区域获得了

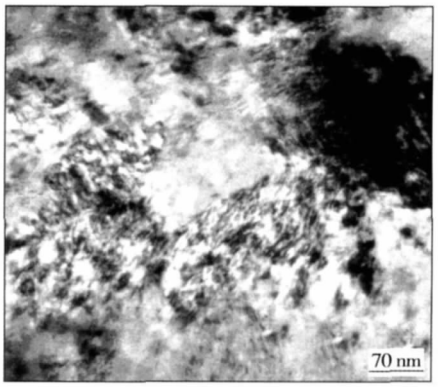

图 2 冲击处理表面组织的高分辨透射电镜明场像
Fig. 2 TEM bright field image with UIT

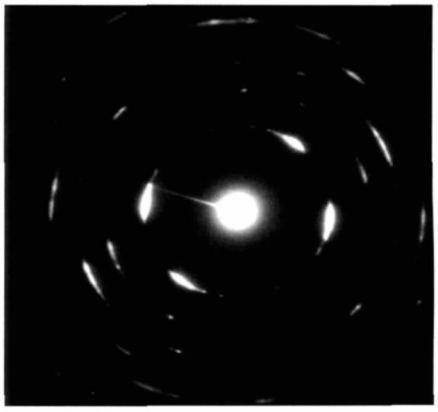

图 3 选区电子衍射花样
Fig. 3 Selected area electron diffraction pattern

纳米组织，晶粒尺寸小于 100 nm. 晶粒趋向呈随机分布，如图 3 所示. 同时在表层组织中形成了大量的位错，位错缠结形成位错墙和位错胞，如图 4 所示. 在进行超声冲击时，冲击针来回冲击材料表面，致使材料中的很多位错开动，即使是处于同一晶粒中，也发生多个滑移系开动. 位错的交互作用除了发生于滑移系之内，还在不同的滑移系之间发生，即

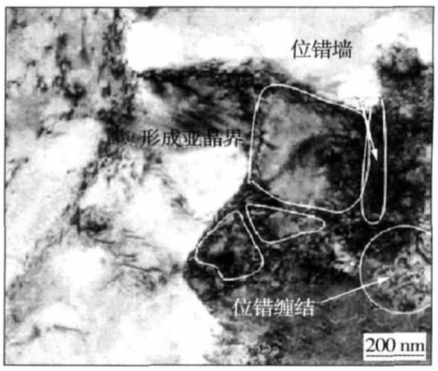

图 4 UIT 后材料表面的位错缠结、位错墙和亚晶
Fig. 4 Dislocation tangle, wall and sub-grain after UIT

位错不仅与此前处于已激活滑移系上的位错交互作用,还与之前静止的位错交互作用. 与其它一些诸如等通道角挤压法和滚压技术等简单的塑性变形技术相比,超声冲击技术可通过形成高致密度的位错缠结和位错墙而更有效地细化原始的粗晶粒.

3.2　疲劳试验结果及分析

16MnR 十字接头疲劳试验结果如表 2 和表 3 所示,相应的对比 S－N 曲线见图 5.

表 2　焊态十字接头试验结果

Table 2　Fatigue test results of welded cross joint

试样编号	最大应力 σ_{max} /MPa	疲劳寿命 N(10^6 周次)	断裂位置
1	200	0.198	焊趾
2	190	0.567	焊趾
3	180	0.886	焊趾
4	175	0.767	焊趾
5	160	1.168	焊趾
6	155	2.465	焊趾
7	150	3.583	焊趾

表 3　冲击态十字接头试验结果

Table 3　Fatigue test results of UIT cross joint

试样编号	最大应力 σ_{max} / MPa	疲劳寿命 N(10^6 周次)	断裂位置
1	300	0.114	焊趾
2	290	0.236	焊趾
3	280	0.539	焊趾
4	250	0.803	焊趾
5	240	1.609	焊趾
6	230	2.574	焊趾

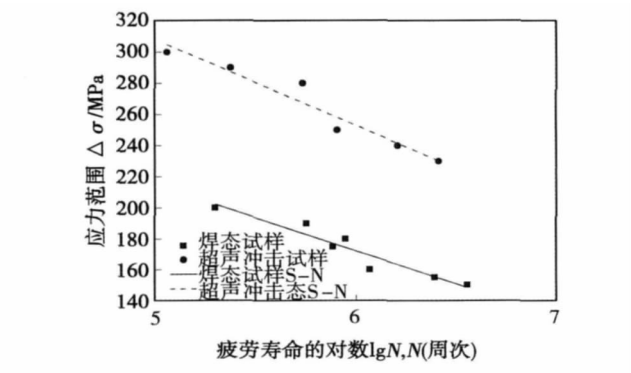

图 5　十字接头对比 S－N 曲线

Fig. 5　S－N curves of cross joints

16MnR 焊态十字接头的 S－N 曲线方程为 $\lg N = 26.76 - 9.29 \lg\sigma_{max}$; 冲击态接头的 S－N 曲线方程为 $\lg N = 32.54 - 11.05 \lg\sigma_{max}$. 曲线拟合参数见表 4 所示,以 2×10^6 疲劳寿命下的应力表征焊接接头的条件疲劳极限,见表 4.

表 4　疲劳试验数据统计结果

Table 4　Statistical results of fatigue test data

处理状态	拟合常数 m	拟合常数 C	疲劳极限 p/MPa
焊态	9.29	5.748×10^{26}	158
冲击态	11.05	3.481×10^{32}	236

图 5 为十字接头对比 S－N 曲线. 观察图 5 可以发现,在相同应力水平下,焊态试样疲劳寿命远低于超声冲击态试样; 在相同疲劳寿命条件下,超声冲击态试样的疲劳强度均远高于焊态试样. 通过对比表 4 中超声冲击态试样与原始焊态试样疲劳寿命为 2×10^6 下获得的条件疲劳极限值发现,超声冲击态十字接头与焊态接头相比,条件疲劳极限提高了 49%.

十字接头试样超声冲击前后均断裂于焊趾处,见图 6 所示. 这是因为焊趾是接头应力集中比较严重的地方. 降低焊趾处的应力集中,有利于焊接接头疲劳性能的提高. 由于焊趾处应力集中程度比较大,即使经过超声冲击处理,焊趾区依然是接头的薄弱环节,接头几何形状突变在焊趾处形成的应力集中是影响接头疲劳性能的一个重要因素.

图 6　十字接头断裂位置

Fig. 6　Fracture position of cross joint

超声冲击处理提高焊接接头疲劳性能的一个重要原因就是降低了焊趾处应力集中程度. 经超声冲击处理后,焊趾表面产生了一定范围的塑性变形层,表层晶粒得到了细化,焊趾部位变成平滑过渡,降低了焊接接头承载时的应力集中程度. 此外,对超生冲击前后焊趾表面的残余应力进行了测量,其纵向残余应力数值分别为 247 MPa 和 －263 MPa,超声冲击不仅能够降低焊接接头的残余应力,甚至将残余拉应力转化成残余压应力. 这些因素均有助于提高焊接接头疲劳性能.

为了获得在相同应力水平条件下焊态试样和冲击态试样的疲劳寿命变化情况,将表 2 和表 3 中相应的数据按方程 $S^mN = C$ 拟合(参数如表 4 所示) ,分别得出焊态试样在疲劳寿命为 10^5 周次时所对应

应力水平条件下冲击态试样的疲劳寿命以及冲击态试样在疲劳寿命为 10^7 周次时所对应应力水平条件下焊态试样的疲劳寿命，结果列于表5.

表5 超声冲击前后疲劳寿命对比

Table 5 Comparison between treated and un-treated specimens

处理状态	最大应力 σ_{max}/MPa	疲劳寿命 N(周次)
焊态	219	1×10^5
冲击态	219	4.57×10^6
焊态	205	1.93×10^5
冲击态	205	1×10^7

对比表5中焊态和冲击态试样在相同应力水平下的疲劳寿命可知，经超声冲击处理的十字接头的疲劳寿命是焊态接头的45～52倍. 超声冲击能够较大幅度地延长16MnR焊接十字接头的疲劳寿命. 超声冲击技术在改善转向架焊接接头疲劳性能方面具有广阔的应用前景.

4 结 论

(1) 16MnR十字接头超声冲击前后的S－N曲线方程分别为 $\lg N = 26.76 - 9.29\lg\sigma_{max}$ 和 $\lg N = 32.54 - 11.05\lg\sigma_{max}$. 在相同应力水平下，焊态试样疲劳寿命远低于冲击态试样；在相同疲劳寿命条件下，冲击态试样的疲劳强度均远高于焊态试样.

(2) 焊态十字接头的条件疲劳极限为158 MPa；冲击态接头的条件疲劳极限为236 MPa. 条件疲劳极限提高了49%.

(3) 16MnR十字接头经超声冲击处理后，焊趾表面晶粒得到细化，降低了焊接接头的应力集中程度. 16MnR十字接头经过超声冲击处理后疲劳寿命延长了45～52倍，超声冲击处理在提高16MnR十字接头疲劳性能方面具有显著的效果.

参考文献：

[1] Haagensen P J, Stamikov E S, Lopez-Martinez L. Introductory fatigue tests on welded joint in high strength steel and aluminum improved by various methods including ultrasonic impact treatment (UIT) [R]. IIW Doc. XIII－1748－98.

[2] 李 东，陈怀宁，刘 刚，等. SS400钢对接接头表面纳米化及其对疲劳强度的影响 [J]. 焊接学报，2002，23(2)：18－21.
Li Dong, Chen Huaining, Liu Gang. Surface nanocrystaillzation of SS400 steel butt welded joint and its effect on the fatigue strength [J]. Transactions of the China Welding Institution, 2002, 23(2): 18－21

[3] 饶德林，陈立功，倪纯珍，等. 超声冲击对焊接结构残余应力的影响 [J]. 焊接学报，2005，26(4)：48－50.
Rao Delin, Chen Ligong, Ni Chunzhen, *et al*. Effect of ultrasonic impact treatment on residual stress of welded structure [J]. Transactions of the China Welding Institution, 2005, 26(4): 48－50.

[4] 王东坡，霍立兴，张玉凤，等. 提高焊接接头疲劳强度的超声波冲击法 [J]. 焊接学报，1999，20(3)：158－163
Wang Dongpo, Huo Lixing, Zhang Yufeng, *et al*. Ultrasonic peening method to improve fatigue strength of welded joint [J]. Transactions of the China Welding Institution, 1999, 20(3): 158－163

[5] 李 强，刘志明，缪龙秀，等. 高速客车转向架残余应力的试验研究 [J]. 试验力学，1999，14(2)：260－266.
Li Qiang, Liu Zhiming, Miao Longxiu, *et al*. Research on the residual stresses in bogie frames of high speed passenger car [J]. Journal of Experimental Mechanics, 1999, 14(2): 260－266

[6] 陶传琦，史春元，朱 平. 铁路客车转向架药芯焊丝MAG焊接头的疲劳性能 [J]. 焊接，2004(10)：19－21.
Tao Chuanqi, Shi Chunyuan, Zhu Ping. Study on fatigue properties of flux cored wire mag welded joint in bogie of passenger train [J]. Welding & Joining, 2004(10): 19－21

[7] 郭 豪，史春元，丁成钢，等. 基于TIG电弧重熔的焊后复合处理工艺改善T形接头疲劳强度的研究 [J]. 焊接，2008(2)：23－26.
Guo Hao, Shi Chunyuan, Ding Chengang, *et al*. T joints fatigue strength improving by hybrid heat treatment process after tungsten inert-gas arc remelting [J], Welding & Joining, 2008(2): 23－26.

[8] 崔晓芳，马 君，兆文忠. 高速动力车转向架构架焊接变形的数值分析研究 [J]. 铁道学报，2004，26(3)：31－35.
Cui Xiaofang, Ma Jun, Zhao Wenzhong. Numerical aimulation study of welding deformation in the bogie frame of the high-speed locomotive [J]. Journal of the China Railway Society, 2004, 26(3): 31－35

[9] Hobbacher A. XⅢ-1539-96/XV-845-96 Recommendations on fatigue design of welded joints and components [S]. Paris: International Institute of Welding, 2002.

作者简介： 何柏林，男，1962年出生，博士，教授，硕士研究生导师. 主要从事焊接结构强度与断裂方面的科研和教学工作. 发表论文70余篇. Email: hebolin@163.com

ture on inner surface of the pipe, was negative for one given molten pool. With the increase of pressure, the radial deformation of the node became positive and the radial deflection increased linearly. However, when the pressure exceeded a certain value, the linear change vanished and the radial deformation increased severely. For different molten pool sizes, when the penetration and pressure remained constant, the less the width and length of molten pool, the higher the instability temperature. When the penetration and the highest temperature on the inner surface of the pipe remained unchanged, the less the width and length of molten pool, the higher the instability pressure.

Key words: in-service welding; burn-through; molten pool size; temperature field

Numerical simulation of residual stress in diffusion bonded TiAl/Ti/GH99 alloy joint LI Haixin[1,2], LIN Tiesong[1], HE Peng[1], FENG Jicai[1] (1. State Key Laboratory of Advanced Welding and Joining, Harbin institute of Technology, Harbin 150001, China; 2. Shandong Provincial Key Laboratory of Special Welding Technology, Institute of Oceanographic Instrumentation, Shandong Academy of Sciences, Qingdao 266001, China). pp 38 - 42

Abstract: Finite element method was used to calculate the residual stress that developed during cooling from joining temperature while diffusion bonding TiAl-based intermetallics to Ni-based alloy with Ti interlayer. The effect of bonding temperature on the distribution of stress and joint size was investigated. The results show that the residual stress concentrated at the interfaces of Ti/GH99 and Ti/TiAl. Especially, the maximum residual stress was higher at the Ti/GH99 interface than at the Ti/TiAl interface. When the bonding temperature decreased, the distribution of stress in the joint was almost constant, while the maximum residual stress decreased. By comparing the simulated and experimental results, it was found that the simulated results agreed well with the experimental results.

Key words: TiAl-based alloy; Ni-based alloy; diffusion bonding; numerical simulation

Effect of aging on the interface and properties of SnAgCu/SnAgCu-TiO_2 solder joints ZHANG Liang[1,2,3], TU K N[3], GUO Yonghuan[1], HE Chengwen[1], ZHANG Jian[1] (1. Mechanical and Electrical Engineering Institute, Jiangsu Normal University, Xuzhou 221116, China; 2. Provincial Key Laboratory of Advanced Welding, Jiangsu University of Science and Technology, Zhenjiang 212003, China; 3. Department of Materials Science and Engineering, University of California, Los Angeles 90024, USA). pp 43 - 46

Abstract: The interface reaction between the Cu substrate and two lead-free solders of SnAgCu and SnAgCu-TiO_2 was investigated, and the growth of intermetallic compounds (IMCs) and mechanical properties of solder joints during aging at 140 ℃ were analyzed systematically. The results indicate that Cu_6Sn_5 was detected at the as-soldered interface, and aging at 140 ℃ resulted in the growth of IMCs. Moreover, it was found that the thickness of IMCs was proportional to the square root of aging time. When the aging time was 300 h, Cu_3Sn appeared at the interface, and the results show that the addition of TiO_2-nanoparticles could inhibit the growth of IMCs. In addition, after analyzing the mechanical properties of solder joints, it was found that with the development of aging time, the average tensile force decreased obviously, and the mechanical properties of the joint soldered with SnAgCu-TiO_2 were higher than that with SnAgCu.

Key words: lead-free solders; interface reaction; intermetallic compound; mechanical property

Self-adapting detection of cycle stages of the current waveform in DP-GMAW process GAO Liwen[1], XUE Jiaxiang[2], CHEN Hui[2], LIN Zhihui[2], LIANG Yongquan[2] (1. School of Medical Information Engineering, Guangzhou University of Chinese Medicine, Guangzhou 510006, China; 2. School of Mechanical and Automotive Engineering, South China University of Technology, Guangzhou 510640, China). pp 47 - 50

Abstract: Detection of cycle stages of the current waveform in DP-GMAW process is the precondition for quantitative feature extraction and power supply evaluation. However, the wide variety of DP-GMAW modulations results in the large difficulties for detection, and related achievements have not been reported. This paper put forward a self-adapting detection method based on the average local current. First, the local time range was estimated, which was followed by the calculation of the average local current sequence. Then, according to the sequence, the double-threshold value method was applied to marking the pulse trains. Finally, each pulse train was subdivided into cycle stages. Tests show that with the above method, five typical types of waveforms during the DP-GMAW process could be accurately divided into phases of pulse train, and the markers of cycle stages within a pulse train were almost all correct, which gave full support to the subsequent feature extraction and other calculations and studies.

Key words: DP-GMAW; cycle stage; detection; local average

Effect of ultrasonic impact on the surface microstructure and fatigue properties of welded cross joint for train bogie HE Bolin[1], YU Yingxia[1], YU Huanghuang[1], JIANG Minhua[1], SHI Jianping[2] (1. Key Laboratory of Ministry of Education for Conveyance and Equipment, East China Jiaotong University, Nanchang 330013, China; 2. China Academy of Railway Sciences, Beijing 100081, China). pp 51 - 54

Abstract: Surface treatment was carried out on the weld toe of welded 16MnR cross joint of train bogie with HJ2-Ⅱ type ultrasonic impact machine. The microstructure of treated surface of weld toe was observed with HRTEM. The fatigue test was performed on both as-welded and treated 16MnR joints with EHF-EM200K2-070-1A type fatigue tester. The experimental results show that the nano-microstructure was obtained in the surface of weld toe and its nearby area. The joints before and after ultrasonic impact fractured through the weld toe. The conditional fatigue limits (2×10^6) of the welded and treated joints were about 158 MPa and 236 MPa, respectively. The conditional fatigue limit

increased by 49% and the fatigue life improved by 45-52 times. The ultrasonic impact treatment has significant effect on improving the fatigue life of 16MnR cross joint for train bogie.

Key words: cross joint; ultrasonic impact; fatigue property; S-N curve; 16MnR steel

Numerical simulation of influence of water depth and flowing speed on thermal process of underwater wet welding

ZHAO Bo[1], WU Chuansong[1], JIA Chuanbao[2], YUAN Xin[2] (1. Key Laboratory for Liquid-Solid Evolution and Processing of Materials (Ministry of Educatong), Shandong University, Jinan 250061, China; 2. Shandong Provincvial Key Laboratory of Special Welding Technology, Institute of Oceanographic Instrumentation, Shandong Academy of Sciences, Qingdao 266001, China). pp 55 - 58

Abstract: The pressure, shape and thermal density of a welding arc will change under high-pressure and strong-cooling underwater environment, so will the heat exchange on the workpiece surface. In this paper, a FEM model of the thermal process of underwater wet gas metal arc welding was established using SYSWELD. Two remarkable characteristics of underwater wet welding-the water compressing action on the arc and the enhanced heat loss caused by the surrounding water-were considered in the model by adjusting the heat sources and convection coefficient on the workpiece surface. Then thermal cycles and weld pool profiles under different water depths and different water flowing speeds were obtained. The calculated results show that the weld pool became deeper and narrower in deeper water, and so did the profiles of the isotherms. And the results also revealed that the weld pool and profiles of isotherms became narrower and shallower when the water flowing speed increased.

Key words: underwater wet welding; temperature field; FEM; heat source model

Brazing Si_3N_4 ceramic with Ag-Cu-Ti + Mo composite filler

HE Yanming, WANG Xing, WANG Guochao, WANG Tianpeng, LIU Chunfeng, ZHANG Jie (School of Materials Science and Engineering, Harbin Institute of Technology, Harbin 150001, China). pp 59 - 62

Abstract: A commercial Ag-Cu-Ti alloy with Mo particles reinforcement was introduced for joining Si_3N_4 ceramic. The effect of Mo content on the microstructure and flexural strength of the resultant joints was investigated by SEM, TEM and nanoindentation. The results indicate that a compact reaction layer consisting of TiN and Ti_5Si_3 formed at the Si_3N_4/filler interface. The central part of the joint was composed of Ag-based solid solution, Cu-based solid solution and Mo particles together with Ti-Cu intermetallics. The modulus and hardness of Ti-Cu intermetallics and the brazing alloy in the joint were measured by nanoindentation. With increasing the Mo particles content in the joint, the thickness of reaction layer decreased while the amount of Ti-Cu intermetallics in the brazed layer increased. In addition, Ag- and Cu-based solid solutions in the brazed layer became finer. The maximal bending strength reached 429.4 MPa while incorporating 15vol.% Mo particles, and the joint strength was 114.7% higher than that without adding Mo particles.

Key words: Si_3N_4 ceramic; brazing; Ag-Cu-Ti + Mo composite filler; nanoindentation; mechanical property

Effects of secondary phases on stress corrosion property of friction stir welded seam of 7A52 aluminum alloy under different strain rates

ZHAO Junjun[1], LI Qi[2], CAI Zhihai[1], ZHANG Ping[1] (1. Department of Equipment Remanufacture Engineering, Academy of Armored Forces Engineering, Beijing 100072, China; 2. Department of Mechanical Engineering, Academy of Armored Forces Engineering, Beijing 100072, China). pp 63 - 66, 75

Abstract: The effects of secondary phases on stress corrosion property of friction stir welded (FSW) seam of 7A52 aluminum alloy were investigated with SEM-EDS during low stress rate test (SSRT). The experimental results indicate that the stress corrosion cracking (SCC) occurred on the retreating side of HAZ in FSW seam in 3.5% NaCl solution. The fracture position was corresponding to the position of minimum microhardness value in FSW seam. The SCC susceptibility of FSW seam was highest at strain rate of 1×10^{-6} s^{-1} and lowest at 1×10^{-5} s^{-1}. Different secondary phases had different effects on the initiation and growth of stress corrosion cracks. Al9Fe0.84Mn2.16Si easily induced the initiation and growth of cracks, however, the pitting resulted from the dissolved Mg_2Si could only initiate small cracks.

Key words: 7A52 aluminum alloy; FSW seam; stress corrosion cracking; secondary phase

New equipment and method for measuring welding residual stress in Francis runner

CHENG Guangfu, WEI Song, WEN Daowei, LI Zheng (State Key Laboratory of Hydro-Power Equipment, Harbin Institute of Large Electrical Machinery, Harbin 150040, China). pp 67 - 70

Abstract: The high welding residual stress in the welded joint in the outlet of blade is one of the major reasons leading to the fatigue failure of Francis turbine runners. The welding residual stress test in as-welded and after post-weld heat treatment has been the necessary process during the manufacture of the runner. The test precision and efficiency have an important influence on the manufacture quality and schedule of runner. According to the structural characteristics of the runner, new test equipment was developed, and the welding residual stress test method for Francis runner was determined. The experimental results show that the test results could truly reflect the distribution of welding residual stress in the runner before and after heat treatment. The new test equipment and method could be applied to the test of welding residual stress in Francis runner with high precision and efficiency.

Key words: Francis runner; welding; residual stress; test

Double closed-loops control for arc length and current in consumable double electrode gas metal arc welding process

ZHU Ming[1], FAN Ding[1], SHI Yu[1], HUANG Jiankang[1], ZHANG Yuming[2] (1. Key Lab of Non-Ferrous Metal Alloys, The Ministry of Education, Lanzhou University of Technology, Lanzhou 730050, China; 2. Center for Manufacturing, Universi-